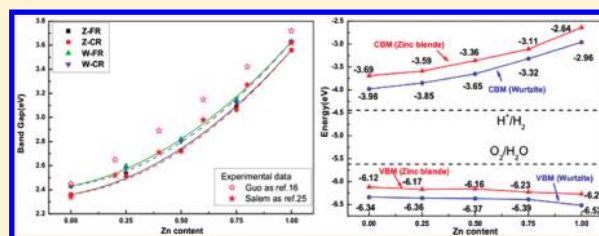


Hybrid Functionals Study of Band Bowing, Band Edges and Electronic Structures of $\text{Cd}_{1-x}\text{Zn}_x\text{S}$ Solid Solution

Jian-Chun Wu,[†] Jianwei Zheng,^{*,‡} Chelsey L. Zacherl,[§] Ping Wu,[‡] Zi-Kui Liu,[§] and Rong Xu[†][†]School of Chemical and Biomedical Engineering, Nanyang Technological University, 62, Nanyang Drive, Singapore 637459[‡]Institute of High Performance Computing, 1 Fusionopolis Way, #16-16 Connexis, Singapore 138632[§]Department of Materials Science and Engineering, The Pennsylvania State University, University Park, Pennsylvania 16802, United States

ABSTRACT: We have systematically studied band bowing, band edges, and electronic properties of both zinc-blende and wurtzite $\text{Cd}_{1-x}\text{Zn}_x\text{S}$ solid solutions by using a special quasirandom structures approach combined with hybrid DFT calculations. Hybrid DFT gives a more accurate description of the lattice constants, formation enthalpies, and electronic structures of the parent semiconductors than standard DFT. Alloying CdS with ZnS causes a downward band bowing that is dominated by volume deformation. The conduction- and valence- band edges straddle the redox potentials of ($\text{O}_2/\text{H}_2\text{O}$) and (H^+/H_2) over the whole Zn concentration range. The high photocatalytic activity of $\text{Cd}_{1-x}\text{Zn}_x\text{S}$ is due to the elevation of the conduction band minimum (CBM). The optimal Zn content is around 0.5, determined as a result of balancing the elevation of the CBM and the widening of the band gap. The valence bandwidth increases with Zn content and thus raises the mobility of photogenerated holes, which may be related to photocorrosion and lead to the leaching of Zn in $\text{Cd}_{1-x}\text{Zn}_x\text{S}$ photocatalyst during water splitting.



INTRODUCTION

Cadmium sulfide (CdS) and zinc sulfide (ZnS) are two widely studied metal sulfides for photocatalytic water splitting.^{1–4} CdS is able to harvest visible light at wavelengths of <510 nm due to its small band gap (~ 2.4 eV). As it lacks active sites for hydrogen evolution,⁵ it is essential to deposit Pt or another noble metal on its surface to act as a cocatalyst.^{6–9} On the other hand, ZnS has a wide band gap of ~ 3.6 eV and is highly active for H_2 production under UV light irradiation even without a metal cocatalyst.^{10,11} Transition metal (Ni and Cu) doped ZnS was found to be able to produce H_2 under visible light irradiation.^{12–14} However, the photocatalytic activity is very low.

Recently, it has been reported that CdS is able to form a solid solution with ZnS through various synthesis methods.^{15–28} The band gap of $\text{Cd}_{1-x}\text{Zn}_x\text{S}$ solid solution is tunable and the photocatalytic activity was significantly improved. The highest H_2 evolution rate was reported to be $2640 \mu\text{mol h}^{-1} \text{g}^{-1}$ at $\lambda \geq 420$ nm for $\text{Cd}_{0.44}\text{Zn}_{0.56}\text{S}$ alloy without a cocatalyst,¹⁷ which is about 33 times higher than that of CdS.

To understand the structural and electronic properties of $\text{Cd}_{1-x}\text{Zn}_x\text{S}$ solid solutions, theoretical studies are desirable. Few theoretical papers have appeared in the literature until recently. Both Noor et al. and Koloğlu et al. used ordered crystal structures to represent zinc-blende $\text{Cd}_{1-x}\text{Zn}_x\text{S}$ solid solution and performed standard density functional theory (DFT) calculations.^{29,30} There is no solid experimental evidence to support ordered $\text{Cd}_{1-x}\text{Zn}_x\text{S}$ crystal structures. Second, the calculated band gap values by GGA and LDA are rather different from the experimental data: 0.9 eV (GGA) and 1.26 eV (LDA) versus

experimental values of 2.37 eV for CdS; 2.0 eV (GGA) and 1.74 eV (LDA) versus 3.54 eV for ZnS.

Herein, we report a hybrid DFT study of the special quasirandom structures (SQSs) of $\text{Cd}_{1-x}\text{Zn}_x\text{S}$ solid solution in either the zinc-blende or wurtzite crystal type. It is well-known that an SQS is able to mimic the disordered structures of a completely random solid solution by creating a periodic structure of 8–32 atoms with a similar correlation function to the random solution for the first several nearest neighbor shells.^{31,32} The properties obtained by relaxing these structures, such as mixing enthalpies, optical bowing parameters, and lattice parameters, agree well with experimental values.^{31–36} Moreover, hybrid DFT provides a more accurate description of the band gap of the two materials, which is essential to the study of a $\text{Cd}_{1-x}\text{Zn}_x\text{S}$ solid solution. Furthermore, we calculate the positions of valence- and conduction-band edges relative to a vacuum following the method reported by Moses et al.,^{37,38} which enables us to align the positions with the redox potentials of ($\text{O}_2/\text{H}_2\text{O}$) and (H^+/H_2) and is helpful to understand the effect of Zn in the $\text{Cd}_{1-x}\text{Zn}_x\text{S}$ solid solution.

COMPUTATIONAL DETAILS

SQS. 16-mixing-atom binary special quasirandom structures (A_{1-x}B_x) at $x = 0.25, 0.5$, and 0.75 for fcc and hcp structures were

Received: May 24, 2011

Revised: September 3, 2011

Published: September 08, 2011

Table 1. Lattice Vectors and Atomic Positions of 32-Atom SQS Supercells for Zinc-Blende $A_{1-x}B_xS$ Solid Solution with 16 Cations and 16 Anions^a

$x = 0.25$				$x = 0.5$			
lattice vectors				lattice vectors			
$\begin{pmatrix} a_0/2 & a_0/2 & -a_0 \\ 0 & -3a_0/2 & -a_0/2 \\ -2.0a_0 & a_0/2 & -a_0/2 \end{pmatrix}$				$\begin{pmatrix} a_0 & -a_0/2 & -a_0/2 \\ 0 & a_0 & -a_0 \\ a_0 & 3a_0/2 & 3a_0/2 \end{pmatrix}$			
0.50000	0.875000	0.125000	A	0.2500	0.2500	0.2500	A
0.25000	0.187500	0.312500	A	0.2500	0.7500	0.2500	A
0.00000	0.500000	0.500000	A	0.7500	0.5000	0.2500	A
0.50000	0.625000	0.375000	A	0.2500	0.0000	0.7500	A
0.50000	0.375000	0.625000	A	0.0000	0.2500	0.5000	A
0.75000	0.812500	0.687500	A	0.5000	0.7500	0.0000	A
0.00000	0.250000	0.750000	A	0.0000	0.5000	0.0000	A
0.25000	0.937500	0.562500	A	0.0000	0.0000	0.0000	A
0.75000	0.562500	0.937500	A	0.5000	0.5000	0.5000	B
0.25000	0.687500	0.812500	A	0.7500	0.0000	0.2500	B
0.50000	0.125000	0.875000	A	0.5000	0.0000	0.5000	B
0.00000	0.000000	0.000000	A	0.2500	0.5000	0.7500	B
0.75000	0.312500	0.187500	B	0.0000	0.7500	0.5000	B
0.25000	0.437500	0.062500	B	0.7500	0.2500	0.7500	B
0.00000	0.750000	0.250000	B	0.7500	0.7500	0.7500	B
0.75000	0.062500	0.437500	B	0.5000	0.2500	0.0000	B
0.68750	0.828125	0.296875	S	0.5625	0.7500	0.1875	S
0.93750	0.515625	0.109375	S	0.5625	0.2500	0.1875	S
0.18750	0.953125	0.171875	S	0.8125	0.5000	0.4375	S
0.93750	0.765625	0.859375	S	0.8125	0.0000	0.4375	S
0.43750	0.890625	0.734375	S	0.0625	0.5000	0.1875	S
0.68750	0.578125	0.546875	S	0.3125	0.7500	0.4375	S
0.93750	0.265625	0.359375	S	0.0625	0.0000	0.1875	S
0.18750	0.703125	0.421875	S	0.3125	0.2500	0.4375	S
0.43750	0.390625	0.234375	S	0.5625	0.5000	0.6875	S
0.68750	0.078125	0.046875	S	0.8125	0.7500	0.9375	S
0.43750	0.640625	0.984375	S	0.5625	0.0000	0.6875	S
0.68750	0.328125	0.796875	S	0.8125	0.2500	0.9375	S
0.93750	0.015625	0.609375	S	0.0625	0.7500	0.6875	S
0.18750	0.453125	0.671875	S	0.0625	0.2500	0.6875	S
0.43750	0.140625	0.484375	S	0.3125	0.5000	0.9375	S
0.18750	0.203125	0.921875	S	0.3125	0.0000	0.9375	S

^a a_0 is the lattice constant in solid solutions.

previously generated and are obtained from the literature.^{33,34} We then add 16 S atoms in the correct Wyckoff positions based on the lattice vectors of the SQSs to create the zinc-blende and wurtzite structures. The S atoms do not mix. The lattice vectors and atomic positions of 32-atom zinc-blende (fcc) and wurtzite (hcp) SQS cells created using this method are listed in Tables 1 and 2, respectively. Once generated, the correlation functions of the newly generated SQS are examined to ensure that it creates an environment that is as close as possible to the random solution for the first several nearest neighbor shells.

Relaxation by DFT may affect the symmetry of SQS supercells, especially in the case of large size-mismatch of the constituent

Table 2. Lattice Vectors and Atomic Positions of 32-Atom SQS Supercells for Wurtzite $A_{1-x}B_xS$ Solid Solution with 16 Cations and 16 Anions^a

$x = 0.25$				$x = 0.5$			
lattice vectors				lattice vectors			
$\begin{pmatrix} 3a_0 & -\sqrt{3}a_0 & -2c_0 \\ 0 & \sqrt{3}a_0 & 0 \\ a_0/2 & \sqrt{3}a_0/2 & c_0 \end{pmatrix}$				$\begin{pmatrix} a_0 & \sqrt{3}a_0 & -2c_0 \\ 3a_0/2 & \sqrt{3}a_0/2 & -c_0 \\ 3a_0 & -\sqrt{3}a_0 & -2c_0 \end{pmatrix}$			
0.00000	0.333333	0.00000	A	0.00000	0.333333	0.333333	A
0.25000	0.333333	0.50000	A	0.25000	0.333333	0.583333	A
0.12500	0.833333	0.25000	A	0.50000	0.333333	0.333333	A
0.75000	0.333333	0.50000	A	0.75000	0.333333	0.583333	A
0.62500	0.833333	0.25000	A	0.62500	0.166667	0.041667	A
0.87450	0.833333	0.75000	A	0.62500	0.166667	0.541667	A
0.43750	0.416667	0.37500	A	0.87500	0.166667	0.291667	A
0.31250	0.916667	0.12500	A	0.87500	0.166667	0.791667	A
0.18750	0.416667	0.87500	A	0.25000	0.333333	0.083333	B
0.06250	0.916667	0.62500	A	0.00000	0.333333	0.833333	B
0.93750	0.416667	0.37500	A	0.75000	0.333333	0.083333	B
0.68750	0.416667	0.87500	A	0.50000	0.333333	0.833333	B
0.50000	0.333333	0.00000	B	0.12500	0.166667	0.041667	B
0.37500	0.833333	0.75000	B	0.12500	0.166667	0.541667	B
0.81250	0.916667	0.12500	B	0.37500	0.166667	0.291667	B
0.56250	0.916667	0.62500	B	0.37500	0.166667	0.791667	B
0.453337	0.146683	0.27975	S	0.22025	0.70633	0.24008	S
0.32837	0.64683	0.02975	S	0.22025	0.70633	0.74008	S
0.20337	0.146683	0.77975	S	0.47025	0.70633	0.49008	S
0.07837	0.64683	0.52975	S	0.72025	0.70633	0.24008	S
0.95337	0.146683	0.27975	S	0.47025	0.70633	0.99008	S
0.82837	0.64683	0.02975	S	0.72025	0.70633	0.74008	S
0.70337	0.146683	0.77975	S	0.97025	0.70633	0.49008	S
0.57837	0.64683	0.52975	S	0.97025	0.70633	0.99008	S
0.14088	0.23017	0.15475	S	0.09525	0.53967	0.19842	S
0.64088	0.23017	0.15475	S	0.09525	0.53967	0.69842	S
0.39088	0.23017	0.65475	S	0.34525	0.53967	0.44842	S
0.26588	0.73017	0.40475	S	0.59525	0.53967	0.19842	S
0.01588	0.73017	0.90475	S	0.34525	0.53967	0.94842	S
0.89088	0.23017	0.65475	S	0.59525	0.53967	0.69842	S
0.76588	0.73017	0.40475	S	0.84525	0.53967	0.44842	S
0.51588	0.73017	0.90475	S	0.84525	0.53967	0.94842	S

^a a_0 and c_0 are the lattice constants in solid solutions.

atoms because local relaxation can distort the symmetry of the parent structure.^{33,39} Additionally, in the case of the hcp structures, the hcp SQS have an additional degree of freedom to consider during relaxation compared to the cubic structures, the c/a ratio. Direct relaxation of the hcp structure could result in a loss of symmetry if the angles between the primitive lattice vectors became too distorted during relaxation.³⁶ In this paper, we consider two kinds of relaxation processes with the goal of choosing the lowest energy that still maintains the overall symmetry of the SQS: (i) constrained relaxation, which simultaneously relaxes the volume and the shape of the cell but not the atomic positions and (ii) full relaxation, which relaxes the atomic

positions as well as the volume and the shape of the cell. We use Z, W, CR, and FR to denote zinc-blende, wurtzite structures, constrained, and full relaxations, respectively. Therefore, there are four combinations denoted in our paper: Z-CR, Z-FR, W-CR, and W-FR. For example, Z-CR stands for zinc-blende SQS with constrained relaxation.

We use the convasp code to qualitatively determine if the symmetry of the SQS supercells has been lost during relaxation by performing a radial distribution analysis.⁴⁰ A radial distribution analysis examines, on average, the distance of each atom in a structure to its first, second, third, and so on, nearest neighbors. The goal is to compare the radial distribution function (RDF) of a relaxed structure to the parent structure to see if the frequency of atomic placement remains unperturbed, that is, the structure has retained its symmetry. The radial distribution analysis of each relaxed structures was obtained by counting the number of atoms within increments of 10^{-3} Å, up to the seventh coordination shell. To eliminate high frequency noise, the raw data was scaled and smoothed through Gaussian smearing with a characteristic distance of 0.02 Å.

DFT Calculations. The calculations are performed using the Vienna ab initio Simulation Package (VASP) with projector augmented wave potentials.^{41,42} The generalized-gradient approximation (GGA) with the standard norm conserving Perdew-Burke-Ernzerhof (PBE) and Heyd-Scuseria-Ernzerhof (HSE06) exchange-correlation functionals are employed.^{43,44} The energy cutoff for the plane-wave basis wave functions is 340 eV for all calculations. For pristine CdS and ZnS unit cells, $5 \times 5 \times 5$ and $9 \times 9 \times 9$ Monkhorst-Pack k-point meshes are used for structural relaxation and band gap calculations, respectively. For $\text{Cd}_{1-x}\text{Zn}_x\text{S}$ solid solutions, $2 \times 2 \times 2$ and $3 \times 3 \times 3$ Monkhorst-Pack k-point meshes are used for hybrid DFT structural optimization and density of states (DOS) calculations, respectively. The band gap is estimated by the difference of the Kohn–Sham eigenvalues at Γ ($E_g^{\Gamma-\Gamma}$) because of the direct band gap nature of CdS and ZnS. The band gaps and lattice constants calculated with HSE06, using 30% of Hartree–Fock exchange for pristine CdS and ZnS, agree very well with the experimental values, which is referred as hybrid DFT in the present work.

Band Alignment. We follow the method reported by Moses et al. to calculate the positions of conduction- and valence-band edges relative to the vacuum.^{37,38} To get the so-called “*natural band alignments*”, we need to perform (i) surface calculations, that allow us to use the vacuum potential as a common reference to align the average electrostatic potential in the crystal to the vacuum, and (ii) bulk calculations, which enable us to obtain valence- and conduction-band positions relative to the average electrostatic potential in the crystal. Please refer to refs 37 and 38 for more detail.

We use 12-layer slabs with 20 Å of vacuum. Each m-plane layer should be nonpolar and contain four cations, thus, allowing for calculations on alloys with 25, 50, and 75% Zn content. To test whether this 12-layer slab is thick enough, we perform calculations on a 20-layer slab. The average electrostatic potential difference between these two slabs is only 0.02 eV, showing that 12-layer slab is sufficient.

RESULTS AND DISCUSSIONS

A. Pristine CdS and ZnS. Table 3 lists the lattice constants and band gaps for various pristine CdS and ZnS crystals calculated using standard and hybrid DFT, respectively. The experimental

Table 3. Lattice Constants and Band Gaps of Zinc-Blende and Wurtzite CdS and ZnS Calculated by Standard and Hybrid DFT

zinc-blende	CdS		ZnS	
	<i>a</i> (Å)	<i>E_g</i> (eV)	<i>a</i> (Å)	<i>E_g</i> (eV)
standard-DFT	5.941	1.04	5.450	2.02
hybrid-DFT	5.887	2.36	5.424	3.56
experimental	5.835 ^a	2.37 ^a	5.409 ^b	3.54 ^c

wurtzite	CdS			ZnS				
	<i>a</i> (Å)	<i>c</i> (Å)	<i>u</i>	<i>E_g</i> (eV)	<i>a</i> (Å)	<i>c</i> (Å)	<i>u</i>	<i>E_g</i> (eV)
standard-DFT	4.212	6.835	0.375	1.10	3.853	6.303	0.375	2.08
hybrid-DFT	4.178	6.782	0.375	2.43	3.836	6.275	0.375	3.63
experimental	4.137 ^d	6.714 ^d	0.375 ^d	2.48 ^c	3.811 ^d	6.234 ^d	0.375 ^d	3.70 ^e

^a Ref 45. ^b Ref 46. ^c Ref 47. ^d Ref 48. ^e Ref 49.

Table 4. Formation Enthalpies (ΔH) of Zinc-Blende (Zinc) and Wurtzite (Wurt) CdS and ZnS by Standard DFT and Hybrid DFT

	formation enthalpies ΔH (eV/pair)					
	standard DFT		hybrid DFT		experimental	
	zinc	wurt	zinc	wurt	zinc	wurt
CdS	−1.490	−1.493	−1.584	−1.586		−1.68 ^a
ZnS	−1.831	−1.825	−1.992	−1.982		−2.10 ^b

^a Ref 50. ^b Ref 51.

values are also presented for comparison.^{45–49} It is evident that hybrid DFT gives more accurate results than standard DFT. The band gap values calculated by hybrid DFT are only 0.4~1.9% different from the experimental values while those by standard DFT are at least 56% smaller than the experimental values. The lattice constants computed by hybrid DFT are only 1% larger than the experimental values, while those by standard DFT are 1.5% larger.

Furthermore, we calculate the formation enthalpies of pure CdS or ZnS and the results are listed in Table 4. The formation enthalpies (ΔH) are the energy gain in forming the crystals and given by

$$\Delta H = \mu_{\text{MS}} - (\mu_{\text{M}}^0 + \mu_{\text{S}}^0) \quad (1)$$

where μ_{MS} is the total energy of pure CdS or ZnS and μ_{M}^0 (μ_{S}^0) is the atomic chemical potential of Cd or Zn (sulfur), which are obtained from the corresponding metal crystal (solid α -sulfur). The formation enthalpies calculated by hybrid DFT are more accurate when compared to experimental values than by standard DFT.^{50,51} Therefore, based on the better accuracy, the hybrid DFT method will be adopted to further study the $\text{Cd}_{1-x}\text{Zn}_x\text{S}$ solid solution.

B. $\text{Cd}_{1-x}\text{Zn}_x\text{S}$ Solid Solution. (i). *Constrained versus Full Relaxation.* We consider two kinds of relaxation in this study: (i) constrained relaxation, in which the volume and the shape of the SQS cell are optimized simultaneously, but not the atomic positions; and (ii) full relaxation, in which the atomic positions as well as the volume and the shape of the cell are fully relaxed.

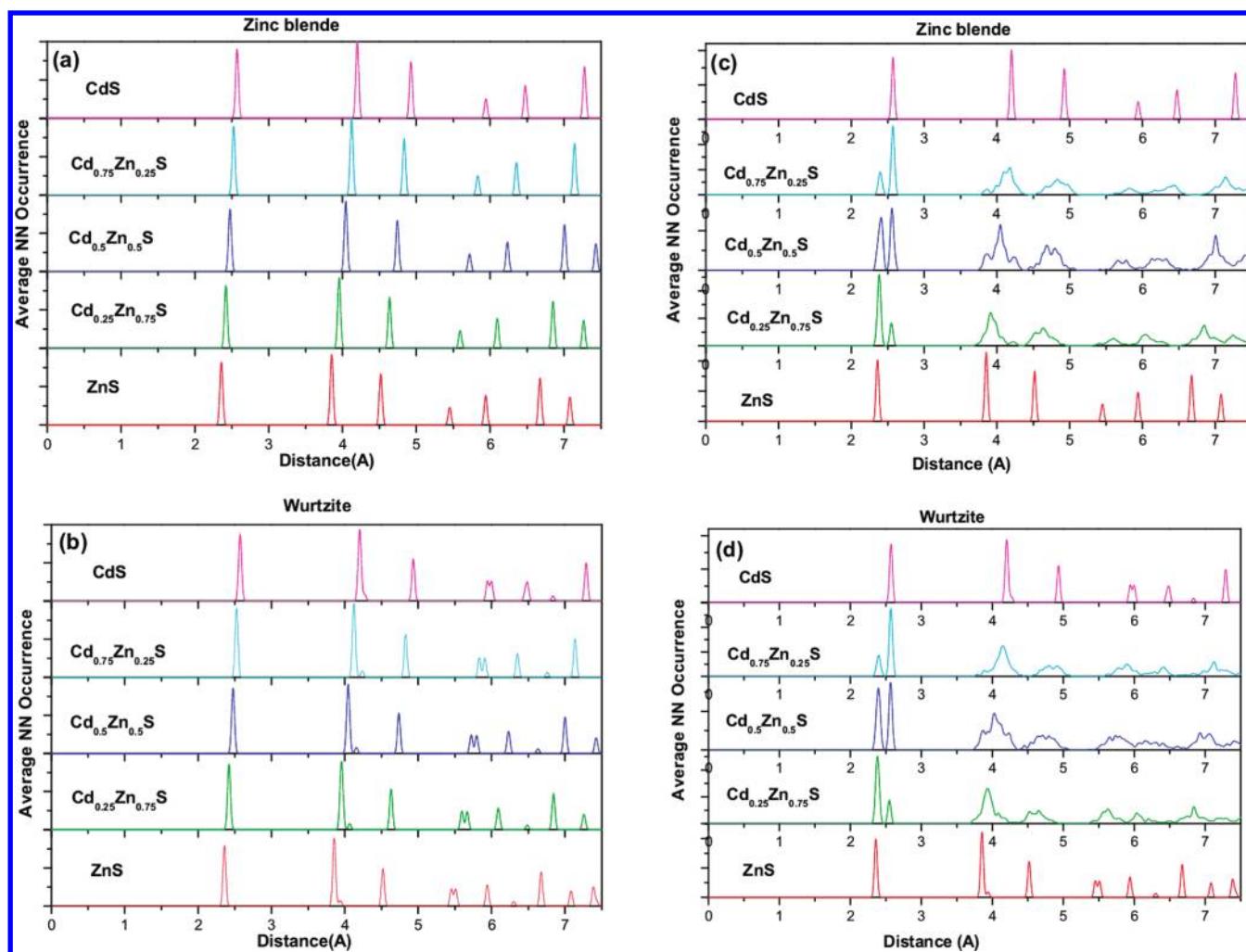


Figure 1. Radial distribution analysis (average nearest neighbor (NN) occurrence vs distance): constrained relaxation: (a) zinc-blende, (b) wurtzite; full relaxation: (c) zinc-blende, (d) wurtzite.

We analyze the symmetry of SQS after relaxation using a radial distribution analysis performed by the convasp code.⁴⁰ As shown in Figure 1a,b, the frequency of RDF peaks of the two SQS after constrained relaxation are very similar to those of the corresponding pristine CdS and ZnS, showing that constrained relaxation does not significantly distort the symmetry of the SQSs. In other words, no noticeable distortions such as peak splitting or peak broadening result from constrained relaxation. This is expected because only the volume of the cell and the lattice vectors changed to relax the structure; the atoms themselves did not move from their initial positions. Another self-consistent observation is the decrease in the location of the first nearest neighbor as the Zn content increases, which is expected from Table 3 showing that the ZnS lattice parameter is smaller than the CdS lattice parameter for both structures. However, as shown in Figure 1c,d, fully relaxing the structures shows some peak broadening and also results in the splitting of the first peak, indicating that the atomic positions have moved. The atom movement is expected because the purpose of the SQS is to create a random “fcc”- or “hcp”-like environment. The splitting of the first peak occurs because the Zn and Cd atoms are different and, thus, will not relax in the same manner. It is observed that the frequency of both the Cd and Zn peak is approximately equal

at $x = 0.5$ and proportional to the Cd and Zn contents in the other fractions, accordingly. While the peak splits due to the two types of mixing atoms that relax differently, this does not show that the structure has completely lost its symmetry. The broadening of the other peaks also occurs because of the two different atom types. What is important is that the peak position relative to that of the parent structure is the same, and there are no peaks that disappear or other peaks that appear after full relaxation.⁵² The peaks do not broaden so much that they are indistinguishable from one another. The deviation of atomic positions from their original lattice positions in zinc-blende structures is slightly larger than that in wurtzite structures. The maximum deviation is <10% for S atoms and <7% for Zn and Cd atoms for both zinc-blende and wurtzite structures after the full relaxation. Based on this qualitative atom position analysis, the conclusion is that the fully relaxed structures can be used to predict the most accurate thermodynamic properties of the solid solution, such as enthalpy of mixing.

Figure 2 shows the enthalpies of mixing of various $\text{Cd}_{1-x}\text{Zn}_x\text{S}$ solid solutions as a function of Cd content. The mixing enthalpies were calculated through the expression

$$\Delta H_{\text{Cd}_{1-x}\text{Zn}_x\text{S}} = E_{\text{Cd}_{1-x}\text{Zn}_x\text{S}} - (1-x)E_{\text{CdS}} - xE_{\text{ZnS}} \quad (2)$$

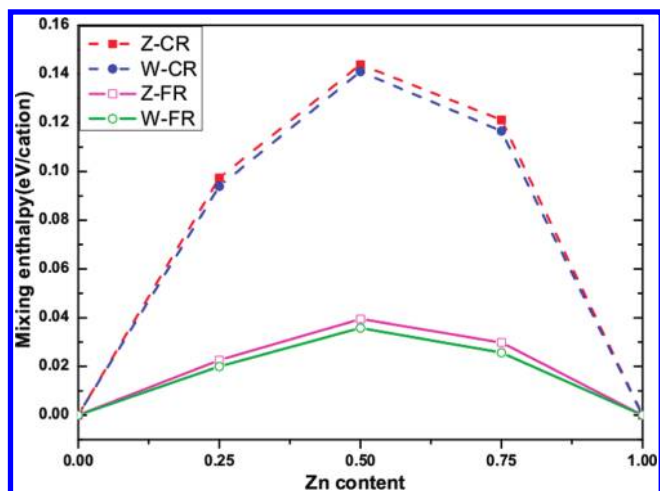


Figure 2. Mixing enthalpies as a function of composition x . Z-CR, Z-FR, W-CR, and W-FR stand for a zinc-blende structure with constrained relaxation, zinc-blende structure with full relaxation, wurtzite structure with constrained relaxation, and wurtzite structure with full relaxation, respectively.

where x is the Zn content, $E_{\text{Cd}_{1-x}\text{Zn}_x\text{S}}$ is the total energy of a $\text{Cd}_{1-x}\text{Zn}_x\text{S}$ SQS, and E_{CdS} and E_{ZnS} are the corresponding reference energies of the pristine CdS and ZnS components, respectively. As can be seen from Figure 2, the mixing enthalpies obtained by constraining the relaxation are more positive than those obtained by full relaxation. This is expected because one fewer parameter contributing to the overall energy was optimized in the DFT calculations when the relaxation was constrained. What is interesting is that the resulting enthalpies of formation of both the constrained and fully relaxed solid solutions are predicted to be slightly positive. A positive enthalpy of mixing indicates the potential for the existence of a miscibility gap and phase separation in the solid solution phase at low temperatures, which is consistent with the physical flattening of the slope of the two-phase zinc-blende and wurtzite mixture in the experimental phases diagrams by Chen et al.⁵⁴ and Federov et al.⁵⁵ around 400 K. One should note, however, that these DFT calculations are performed at 0 K and do not include any entropic effects that stabilize the mixed solution at finite temperatures.

For validation purposes, the enthalpy of mixing results in Figure 2 are compared to the phase diagram of the ZnS–CdS system predicted by Federov et al.⁵⁵ who examined of the phase boundaries through the $\text{Cd}^{2+} \rightarrow \text{Zn}^{2+}$ ion exchange process in a ZnS powder. Based on the experimental phase diagram results, Federov et al. predicted linear temperature dependencies of the enthalpy of mixing for each structure. At temperatures from 300 to 900 K, the enthalpies of mixing as calculated based on their analysis are predicted to be positive. If we compare the room temperature (300 K) enthalpies of mixing from Federov et al. at $x_{\text{Zn}} = 0.5$,⁵⁵ we find them to be 2625 and 3770 J/mol for the zinc-blende and wurtzite structures, respectively. From the SQS results in this work, we predict the enthalpies of mixing to be 3762 and 3569 J/mol for the zinc-blende and wurtzite structures, respectively, agreeing well with the estimations by Federov et al.⁵⁵

To reconcile the 0 K static energy of the system with the Gibbs energy calculated in experiments, one can apply an empirical model of the Gibbs energy as a function of temperature to estimate the nonideal interactions of the solid solution, 0L , the

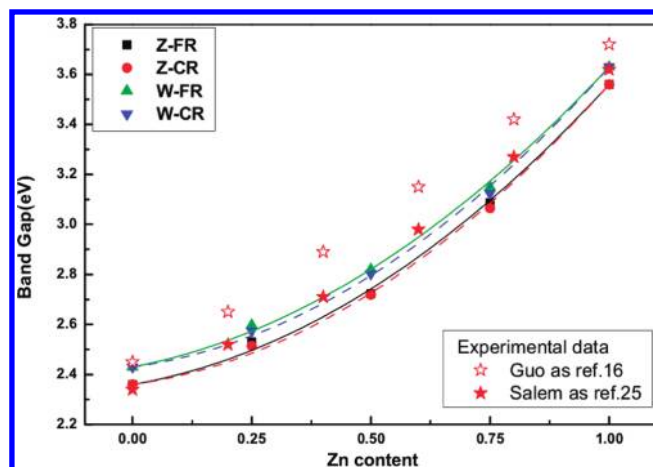


Figure 3. Band gap calculated by hybrid DFT as a function of Zn content.

excess Gibbs energy, through the equation

$$G^{\text{Ex}} = H^{\text{Ex}} - TS^{\text{Ex}} = x_{\text{A}}x_{\text{B}}{}^0L(x_{\text{A}} - x_{\text{B}}) \quad (3)$$

where H^{Ex} and S^{Ex} are the excess enthalpy and entropy, respectively. Under this approximation, the consolute point of the potential miscibility gap in this system, that is, the temperature where the phase separation no longer exists, can be estimated. For a regular solution, the consolute point can be calculated using the following equation⁵³

$$T_{\text{consolute}} = \frac{x_{\text{Zn}}x_{\text{Cd}}L^0}{2R} \quad (4)$$

where R is the gas constant and L^0 is the regular solution interaction parameter evaluated from the enthalpy of mixing from first-principles calculations, that is, 15100 and 14300 J/mol for zinc-blende and wurtzite solutions, respectively, at $x_{\text{Zn}} = 0.5$. The theoretical consolute points thus obtained are around 905 K for the zinc-blende solution and around 860 K for the wurtzite solution. Relative to the phase diagram by Federov et al.,⁵⁵ both of these temperatures fall within the wurtzite region, so it is likely that if a miscibility were to exist, entropic effects would stabilize the solid solution and phase separation would occur at lower temperatures.

(ii). *Band Bowing.* Figure 3 shows the calculated band gap values of various SQS and two sets of experimental values.^{16,25} It is noted that both constrained and full relaxations generate almost the same band gap values. Second, the band gap increases nonlinearly with increasing Zn content. Nonlinearity in an alloy band gap is conventionally expressed as⁵⁶

$$E_{\text{g}}(x) = (1-x)E_{\text{g,CdS}} + xE_{\text{g,ZnS}} - bx(1-x) \quad (5)$$

where $E_{\text{g}}(x)$, $E_{\text{g,CdS}}$, and $E_{\text{g,ZnS}}$ are the band gap energies of $\text{Cd}_{1-x}\text{Zn}_x\text{S}$, CdS, and ZnS, respectively, and b is the bowing parameter. The bowing parameters obtained are 0.94 ± 0.05 , 0.87 ± 0.06 , 0.94 ± 0.05 , and 0.84 ± 0.05 eV for Z-CR, Z-FR, W-CR, and W-FR, respectively. The bowing parameters of the zinc-blende structures are slightly larger than those of the wurtzite structures, which is in accordance with the trend found for the deviation of their atomic positions shown in section (i).

The bowing parameter can be decomposed into three kinds of contributions: volume-deformation (b_{VD}), charge-exchange

Table V. Volume-Deformation (b_{VD}), Charge-Exchange (b_{CE}), and Structural Relaxation (b_{SR}) Contributions to $Cd_{0.5}Zn_{0.5}S$ SQS Optical Bowing (All Values Are in eV)

structure	b	b_{VD}	b_{CE}	b_{SR}
zinc-blende $Cd_{0.5}Zn_{0.5}S$	0.948	0.814	0.150	-0.016
wurtzite $Cd_{0.5}Zn_{0.5}S$	0.837	0.838	0.070	-0.071

(b_{CE}), and structural relaxation (b_{SR}):⁵⁶

$$b = b_{VD} + b_{CE} + b_{SR} \quad (6)$$

The volume deformation contribution represents the relative response of the band structures of CdS and ZnS to hydrostatic pressure and can be calculated by this formula (taking $Cd_{0.5}Zn_{0.5}S$ as an example):⁵⁶

$$b_{VD} = 2[E_{g,CdS} - E_{g,CdS}@V_{Cd_{0.5}Zn_{0.5}S} - CR] - 2[E_{g,ZnS} - E_{g,ZnS}@V_{Cd_{0.5}Zn_{0.5}S} - CR] \quad (7)$$

where $E_{g,CdS}$ and $E_{g,ZnS}$ are the band gap values of pristine CdS and ZnS, respectively, and $E_{g,CdS}@V_{Cd_{0.5}Zn_{0.5}S} - CR$ and $E_{g,ZnS}@V_{Cd_{0.5}Zn_{0.5}S} - CR$ are the band gap values obtained by compressing pristine CdS and dilating pristine ZnS from their equilibrium volumes to the volume of $Cd_{0.5}Zn_{0.5}S$ SQS (constrained relaxation), respectively.

The charge exchange contribution reflects the charge transfer effect and can be calculated by the following formula:⁵⁶

$$b_{CE} = 2E_{g,CdS}@V_{Cd_{0.5}Zn_{0.5}S} - CR + 2E_{g,ZnS}@V_{Cd_{0.5}Zn_{0.5}S} - CR - 4E_{g,Cd_{0.5}Zn_{0.5}S}@V_{Cd_{0.5}Zn_{0.5}S} - CR \quad (8)$$

The structural contribution measures changes upon passing from the unrelaxed SQS supercell to the relaxed SQS supercell, that is, the internal structural relaxation effect. It can be calculated by⁵⁶

$$b_{SR} = 4E_{g,Cd_{0.5}Zn_{0.5}S}@V_{Cd_{0.5}Zn_{0.5}S} - CR - 4E_{g,Cd_{0.5}Zn_{0.5}S}@V_{Cd_{0.5}Zn_{0.5}S} - FR \quad (9)$$

We calculate the total bowing parameter and the three corresponding contributions from the decomposed zinc-blende and wurtzite structures. The results are listed in Table V. As can be seen from the table, the volume-deformation contribution (b_{VD}) dominates the band bowing. The charge-exchange contribution (b_{CE}) and the structural relaxation contribution (b_{SR}) are small. Because the equilibrium lattice constants of the solid solution usually follow Vegard's rule, b_{VD} is expected to be large if the volume deformation potentials of the binary constituents are different. The absolute volume deformation potential for state i can be defined as $a_i^v = dE_i/d \ln v$, which describes the shift of individual energy level E_i with respect to an absolute energy reference in a crystal under a volume (v) deformation. The calculated absolute volume deformation potentials of valence band maximum (VBM) are 0.83 and 0.40 eV for ZnS and CdS, respectively. The absolute volume deformation potentials of conduction band minimum (CBM) are -4.33 and -2.54 eV for ZnS and CdS, respectively.⁵⁷ The large absolute volume deformation potential difference between CdS and ZnS results in the large volume deformation contribution. On the other hand, the electronegativity of Cd (1.69) is very close to that of Zn (1.65).⁵⁰ Hence, the charge-exchange contribution is expected to be small. As the maximum deviation of the atomic positions is

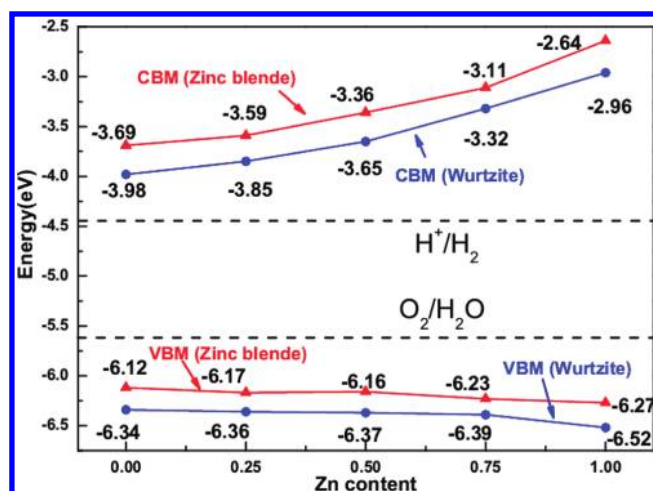


Figure 4. CBM and VBM position with respect to the vacuum level as a function of Zn content. The dash lines indicate the reduction potential of H^+/H_2 (-4.44 eV) and the oxidation potential of O_2/H_2O (-5.67 eV).

<10% for S atoms and <7% for Zn and Cd atoms, it is not surprising that the structural relaxation contribution is also small.

(iii). *Band Edges.* To split water into hydrogen and oxygen, a successful photocatalyst must balance the following crucial factors: absorbance, redox potential, and mobility and lifetime of the photoexcited charge carriers. The conduction band (CB) and valence band (VB) must straddle the redox potential of hydrogen and water while shifting the absorption of the photocatalyst to the visible region by either doping or forming a solid solution. The mobility of photoexcited charge carriers are closely related to the valence bandwidth and the conduction band minimum. The valence bandwidth controls the mobility of holes. The wider the VB, the higher the mobility of the holes. As the generated holes are usually consumed by sacrificial agents, the VB width may not be as important as the CBM for metal sulfide photocatalysts, but VB width may relate to the photocorrosion of the catalyst. The elevation of the CBM can not only provide more reductive photoexcited electrons, but also inhibit electron-hole recombination.⁵⁸ To understand the effect of ZnS in $Cd_{1-x}Zn_xS$ solid solution, it is of interest to calculate the absolute position of VBM and CBM with respect to the vacuum and align them with the redox potentials of (O_2/H_2O) and (H^+/H_2).

Figure 4 shows the calculated conduction- and valence-band edges with respect to the vacuum as a function of Zn content, using the method reported by Moses et al. Our calculated CBM edges for pristine CdS and ZnS are consistent with the experimental flat band potential values: -3.69 eV (wurtzite) and -3.98 eV (zinc-blende) versus -3.88 eV for CdS; -2.64 eV (wurtzite) and -2.96 eV (zinc-blende) versus -2.95 eV for ZnS.⁵⁹ As shown in the figure, the valence- and conduction-bands of $Cd_{1-x}Zn_xS$ solid solution always straddle the redox potentials of (O_2/H_2O) and (H^+/H_2) over the whole Zn content range. With increasing Zn content, the CBM shifts to a more positive level, while the VBM becomes slightly more negative. The maximum uplift magnitude of the CBM edges is 0.98 eV for zinc-blende structures and 1.05 eV for wurtzite structures, while the maximum downshift magnitude of VBM edges is only 0.18 eV for zinc-blende structures and 0.15 eV for wurtzite structures. This indicates that alloying with ZnS mainly influences the conduction band edge. Elevation of the CBM edge significantly

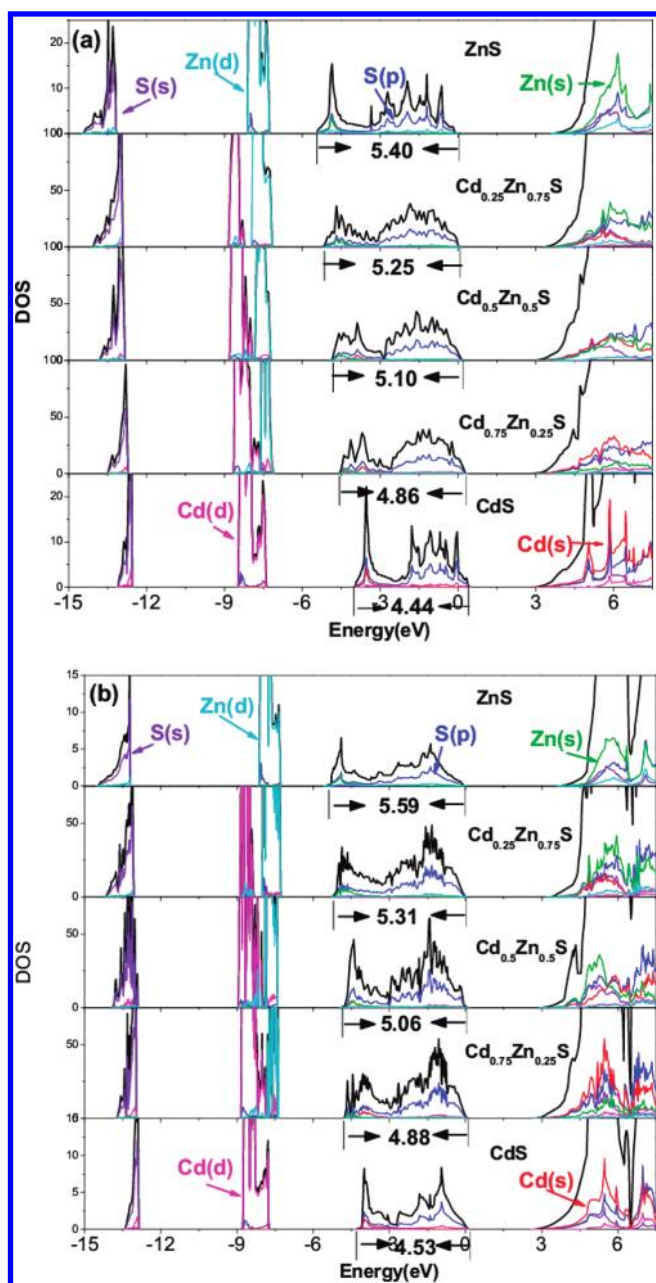


Figure 5. Total and partial density of states. The valence bandwidth is indicated in each figure. The bottom of the conduction band has been magnified 10 \times for clarity.

improves the photocatalytic activity of $\text{Cd}_{1-x}\text{Zn}_x\text{S}$ solid solutions. The photocatalytic activity of $\text{Cd}_{0.44}\text{Zn}_{0.56}\text{S}$ alloy is 33 times higher than that of CdS at $\lambda \geq 420$ nm.¹⁷ However, alloying with ZnS will inevitably widen the band gap. When the Zn content reaches 75%, the band gap is about 3.1 eV, implying that $\text{Cd}_{0.25}\text{Zn}_{0.75}\text{S}$ is not active in the visible light region. Considering these two factors, the optimal Zn content should be around 50%, which agrees well with the experimental observation.¹⁷

IV. Density of States. We now look at the variation of the electronic structures of $\text{Cd}_{1-x}\text{Zn}_x\text{S}$ solid solution with Zn content. The total and partial density of states (DOS) are shown in Figure 5. DOS of pristine CdS and ZnS are also shown for

comparison. As can be seen, for pristine CdS or ZnS, the top of the valence band is dominated by S 3p states and the bottom of the valence band has weak contribution from the 3d states of Zn or 4d states of Cd. Main Zn 3d (Cd 4d) states are located at around $-7.2 \sim -8.1$ eV ($-7.4 \sim -8.5$ eV). Cd 5s or Zn 4s states together with S 3s and 3p states prevail in the bottom of the conduction band. The DOS of $\text{Cd}_{1-x}\text{Zn}_x\text{S}$ solid solution can be seen as the combination of CdS and ZnS. The top of the valence band is still dominated by S 3p states, while Cd 5s, Zn 4s, and S 3p and 3s states dominate the bottom of the conduction band. With increasing Zn content, the magnitude of Zn states increases while the magnitude of Cd states decreases. Two interesting features can be seen from the figure. First, there is only a small change in the position of the main Zn 3d and Cd 4d peaks, implying weak p–d coupling, which explains the small downshift magnitude of the valence band edge well, once it has been alloyed with ZnS. Second, the valence bandwidth gradually increases with increasing Zn content.

The maximum increment of the valence bandwidth is 0.96 eV for zinc-blende structures and 1.06 eV for wurtzite structures. The importance of valence bandwidth has been demonstrated in sulfur-doped graphitic C_3N_4 systems.⁵⁸ The wider the valence bandwidth, the higher the mobility of holes generated by light irradiation. As photogenerated holes are closely related to the photocorrosion of metal sulfide photocatalyst, ZnS may photocorrode more easily than CdS. This may explain the leaching of Zn in $\text{Cd}_{1-x}\text{Zn}_x\text{S}$ nanoparticles during the process of photocatalytic water splitting.⁶⁰

CONCLUSIONS

We have systematically investigated band bowing, band edges and electronic properties of both zinc-blende and wurtzite $\text{Cd}_{1-x}\text{Zn}_x\text{S}$ solid solution by using special quasirandom structures coupled with hybrid DFT calculations. The lattice constants, band gap values, and formation enthalpies of pristine CdS and ZnS obtained by hybrid DFT agree well with the experimental values. Local relaxation slightly lowers the mixing enthalpy and does not influence the band gap values. The downward band bowing was due to the volume deformation contribution. The conduction- and valence-band edges straddle the redox potentials of ($\text{O}_2/\text{H}_2\text{O}$) and (H^+/H_2) over the whole Zn concentration range. Alloying with ZnS raises the conduction band minimum and widens the valence bandwidth. The former drastically improves the photocatalytic activity, while the latter may be responsible for the leaching of Zn in $\text{Cd}_{1-x}\text{Zn}_x\text{S}$ during the process of photocatalytic water splitting.

AUTHOR INFORMATION

Corresponding Author

*Tel.: +65 64191567. Fax: +65 64632536. E-mail: zhengjw@ihpc.a-star.edu.sg.

ACKNOWLEDGMENT

The authors gratefully acknowledge research funding support from the Ministry of Education (MOE) of Singapore (T208B1215) and support received from the Institute of High Performance Computing (A*STAR). C.L.Z. and Z.K.L. are supported by the United States National Science Foundation through the Grant DMR-1006557.

REFERENCES

- (1) Chen, X.; Shen, S.; Guo, L.; Mao, S. S. *Chem. Rev.* **2010**, *110*, 6503–6570.
- (2) Kudo, A.; Miseki, Y. *Chem. Soc. Rev.* **2009**, *38*, 253–278.
- (3) Osterloh, F. E. *Chem. Mater.* **2008**, *20*, 35–54.
- (4) Maeda, K.; Domen, K. *J. Phys. Chem. C* **2007**, *111*, 7851–7861.
- (5) Meissner, D.; Memming, R.; Kastening, B. *J. Phys. Chem.* **1988**, *92*, 3476–3483.
- (6) Jing, D. W.; Guo, L. J. *J. Phys. Chem. B* **2006**, *110*, 11139–11145.
- (7) Jang, J. S.; Joshi, U. A.; Lee, J. S. *J. Phys. Chem. C* **2007**, *111*, 13280–13287.
- (8) Bao, N.; Shen, L.; Takata, T.; Domen, K.; Gupta, A.; Yanagisawa, K.; Grimes, C. A. *J. Phys. Chem. C* **2007**, *111*, 17527–17534.
- (9) Yan, H.; Yang, J.; Ma, G.; Wu, G.; Zong, X.; Lei, Z.; Shi, J.; Li, C. *J. Catal.* **2009**, *266*, 165–168.
- (10) Reber, J. F.; Meier, K. *J. Phys. Chem.* **1984**, *88*, 5903–5913.
- (11) Zeug, N.; Bücheler, J.; Kisch, H. *J. Am. Chem. Soc.* **1985**, *107*, 1459–1465.
- (12) Kudo, A.; Sekizawa, M. *Catal. Lett.* **1999**, *58*, 241–243.
- (13) Kudo, A.; Sekizawa, M. *Chem. Commun.* **2000**, 1371–1372.
- (14) Hamanoi, O.; Kudo, A. *Chem. Lett.* **2002**, 838–839.
- (15) Xu, X.; Lu, R. J.; Zhao, X. F.; Xu, S. L.; Lei, X. D.; Zhang, F. Z.; Evans, D. G. *Appl. Catal., B* **2011**, *102*, 147–156.
- (16) Li, M. T.; Jiang, J. G.; Guo, L. J. *Int. J. Hydrogen Energy* **2010**, *35*, 7036–7042.
- (17) Wang, L.; Wang, W. Z.; Shang, M.; Yin, W. Z.; Sun, S. M.; Zhang, L. *Int. J. Hydrogen Energy* **2010**, *35*, 19–25.
- (18) Zhang, W.; Zhong, Z.; Wang, Y.; Xu, R. *J. Phys. Chem. C* **2008**, *112*, 17635–17642.
- (19) Li, W. J.; Li, D. Z.; Chen, Z. X.; Huang, H. J.; Sun, M.; He, Y. H.; Fu, X. Z. *J. Phys. Chem. C* **2008**, *112*, 14943–14947.
- (20) Wang, W. Z.; Zhu, W.; Xu, H. L. *J. Phys. Chem. C* **2008**, *112*, 16754–16758.
- (21) Zhang, K.; Jing, D. W.; Xing, C. J.; Guo, L. J. *Int. J. Hydrogen Energy* **2007**, *32*, 4685–4691.
- (22) Xing, C. J.; Zhang, Y. J.; Yan, W.; Guo, L. J. *Int. J. Hydrogen Energy* **2006**, *31*, 2018–2024.
- (23) Zhong, X. H.; Feng, Y. Y.; Knoll, W.; Han, M. Y. *J. Am. Chem. Soc.* **2003**, *125*, 13559–13563.
- (24) Wang, W. Z.; Germanenko, I.; El-Shall, M. S. *Chem. Mater.* **2002**, *14*, 3028–3033.
- (25) Salem, A. M. *Appl. Phys. A: Mater. Sci. Process.* **2002**, *74*, 205–211.
- (26) Cheon, J.; Zink, J. I. *J. Am. Chem. Soc.* **1997**, *119*, 3838–3839.
- (27) Nyman, M.; Hampden-Smith, M. J.; Duesler, E. N. *Chem. Vap. Depos.* **1996**, *2*, 171–174.
- (28) Singh, V.; Singh, S. *Czech. J. Phys.* **1976**, *26*, 1161–1166.
- (29) Noor, N. A.; Ikram, N.; Ali, S.; Nazir, S.; Alay-e-Abbas, S. M.; Shaikat, A. *J. Alloys Compd.* **2010**, *507*, 356–363.
- (30) Korozlu, N.; Colakoglu, K.; Deligoz, E. *Phys. Status Solidi* **2010**, *247*, 1214–1219.
- (31) Zunger, A.; Wei, S. -H.; Ferreira, L. G.; Bernard, J. E. *Phys. Rev. Lett.* **1990**, *65*, 353–356.
- (32) Wei, S. -H.; Ferreira, L. G.; Bernard, J. E.; Zunger, A. *Phys. Rev. B* **1990**, *42*, 9622–9649.
- (33) Wolverson, C. *Acta Mater.* **2001**, *49*, 3129–3142.
- (34) Gan, C. K.; Feng, Y. P.; Srolovitz, D. J. *Phys. Rev. B* **2006**, *73*, 235214.
- (35) Shin, D.; Arróyave, R.; Liu, Z. -K. *Phys. Rev. B* **2006**, *74*, 024204.
- (36) Zacherl, C.; Saal, J.; Wang, Y.; Liu, Z. K. *Intermetallics* **2010**, *18*, 2412–2418.
- (37) Mosesa, P. G.; Van de Walle, C. G. *Appl. Phys. Lett.* **2010**, *96*, 021908.
- (38) Mosesa, P. G.; Mao, M.; Yan, Q.; Van de Walle, C. G. *J. Chem. Phys.* **2011**, *143*, 084703.
- (39) Lu, Z. W.; Wei, S. -H.; Zunger, A. *Phys. Rev. B* **1991**, *44*, 3387–3390.
- (40) Morgan, D.; Curtarolo, S.; Ceder, G. <http://burgaz.mit.edu/PUBLICATIONS/codes.php>.
- (41) Kresse, G.; Furthmüller, J. *Phys. Rev. B* **1996**, *54*, 11169–11186.
- (42) Kresse, G.; Furthmüller, J. *Comput. Mater. Sci.* **1996**, *6*, 15–50.
- (43) Perdew, J. P.; Ernzerhof, M.; Burke, K. *J. Chem. Phys.* **1996**, *105*, 9982–9985.
- (44) Heyd, J.; Scuseria, G. E.; Ernzerhof, M. *J. Chem. Phys.* **2003**, *118*, 8207–8215.
- (45) (a) Yu, Y. -M.; Kim, K. -M.; Byung-sung, O.; Lee, K. -S.; Choi, Y. D.; Yu, P. Y. *J. Appl. Phys.* **2002**, *92*, 1162–1164. (b) Yu, Y. -M.; Lee, K. -S.; Byung-sung, O.; Yu, P. Y.; Kim, C. -S.; Choi, Y. D.; Yun, H. -J. *J. Vac. Sci. Technol., A* **2004**, *22*, 324–327.
- (46) Skinner, B. J. *Am. Mineral.* **1961**, *46*, 1399–1411.
- (47) (a) Tran, T. K.; Park, W.; Tong, W.; Kyi, M. M.; Wagner, B. K.; Summers, C. J. *J. Appl. Phys.* **1997**, *81*, 2803–2809. (b) Tran, T. K.; Park, W.; Tong, W.; Kyi, M. M.; Wagner, B. K.; Summers, C. J. *J. Phys. Chem. C* **2010**, *114*, 12099–12103.
- (48) Xu, Y. N.; Ching, W. Y. *Phys. Rev. B* **1993**, *48*, 4335–4351.
- (49) Madelung, O. *Semiconductors: Data Handbook*, 3rd ed.; Springer: New York, 2004; p 221.
- (50) Lide, D. R. *CRC Handbook of Chemistry and Physics*, 86th ed.; CRC Press: New York, 2005; pp 5–8, 12–11, 12–12.
- (51) Masterton, W. L.; Slowinski, E. J.; Stanitski, C. L. *Chemical Principles*; CBS College Publishing: San Francisco, 1977; p 67.
- (52) Kim, D. E.; Manga, V. R.; Prins, S. N.; Liu, Z. -K. *CALPHAD: Comput. Coupling Phase Diagrams Thermochem.* **2011**, *35*, 20–29.
- (53) Hillert, M. *Phase Equilibria, Phase Diagrams, and Phase Transformations: Their Thermodynamic Basis*, 2nd ed.; Cambridge University Press: New York, 2007; pp445–446.
- (54) Chen, W. W.; Zhang, J. M.; Ardell, A. J.; Dunn, B. *Mater. Res. Bull.* **1988**, *23*, 1667–1673.
- (55) Fedorov, V. A.; Ganshin, V. A.; Korkishko, Y. N. *Mater. Res. Bull.* **1993**, *28*, 59–66.
- (56) Bernard, J. E.; Zunger, A. *Phys. Rev. B* **1987**, *36*, 3199–3228.
- (57) Li, Y. H.; Gong, X. G.; Wei, S. -H. *Phys. Rev. B* **2006**, *73*, 245206.
- (58) Liu, G.; Niu, P.; Sun, C.; Smith, S. C.; Chen, Z.; Lu, G. Q.; Cheng, H. -M. *J. Am. Chem. Soc.* **2010**, *132*, 11642–11648.
- (59) Xu, Y.; Schoonen, M. A. A. *Am. Mineral.* **2000**, *85*, 543–556.
- (60) Wang, Y. B.; Wu, J. C.; Zheng, J. W.; Xu, R. *Catal. Sci. Technol.* **2011**, *1*, 940–947.